

A comparison between the P_c and P_{cs} systems

Kan Chen^{1,*}, Zi-Yang Lin^{1,†} and Shi-Lin Zhu^{1‡}

¹*School of Physics and Center of High Energy Physics, Peking University, Beijing 100871, China*

We construct the effective potentials of the P_c and P_{cs} states based on the $SU(3)_f$ symmetry and heavy quark symmetry. Then we perform the coupled-channel analysis of the lowest isospin P_c and P_{cs} systems. The coupled-channel effects play different roles in the P_c and P_{cs} systems. In the P_c systems, this effect gives minor corrections to the masses of the P_c states. In the P_{cs} system, the $\Lambda_c \bar{D}_s - \Xi_c \bar{D}$ coupling will shift the mass of the $P_{cs}(4338)$ close to the $\Xi_c \bar{D}$ threshold. The $\Lambda_c \bar{D}_s^{(*)} - \Xi_c \bar{D}^{(*)}$ coupling will also produce extra P_{cs} states. We discuss the correspondence between the P_c and P_{cs} states. Our results prefer that the $SU(3)$ partners of the observed $P_c(4312)$, $P_c(4440)$, and $P_c(4457)$ in the P_{cs} system have not been found yet.

I. INTRODUCTION

Very recently, the LHCb Collaboration announced the observation of a $P_{cs}(4338)$ signal from the $J/\Psi\Lambda$ mass spectrum in the $B^- \rightarrow J/\Psi\Lambda\bar{p}$ process [1]. The mass and width of this new pentaquark candidate were measured to be

$$M_{P_{cs}} = 4338.2 \pm 0.7 \pm 0.4 \text{ MeV}, \quad (1)$$

$$\Gamma_{P_{cs}} = 7.0 \pm 1.2 \pm 1.3 \text{ MeV}. \quad (2)$$

Meanwhile, the amplitude analysis prefers the $\frac{1}{2}^-$ spin-parity quantum numbers. The central value of the mass of $P_{cs}(4338)$ is above the $\Xi_c \bar{D}$ threshold. Thus, this state can not be directly assigned as the $\Xi_c \bar{D}$ molecular state. However, the authors of Ref. [2] pointed out that the lineshape of this resonance could be distorted from the conventional Breit-Wigner distribution if it lies very close to and strongly couples to the threshold.

Besides the newly observed $P_{cs}(4338)$, the $P_{cs}(4459)$ was observed at LHCb [3] as a candidate of a $\Xi_c \bar{D}^*$ molecular state, which agrees well with the prediction from the chiral effective field theory in Ref. [4]. The strange hidden-charm states were also discussed in Refs. [5–13] and reviewed extensively in Refs. [14–19].

The mass of the $P_{cs}(4459)$ is about 19 MeV below the $\Xi_c \bar{D}$ threshold. In Ref. [20], the author argued that from heavy quark symmetry, the $[\Xi_c \bar{D}]^{1/2^-}$, $[\Xi_c \bar{D}^*]^{1/2^-}$, and $[\Xi_c \bar{D}^*]^{3/2^-}$ channels should share identical potentials and have comparable binding energies. However, the heavy quark symmetry is drastically violated in the charm system due to the rather small charm quark mass. With the assignment of the $P_{cs}(4338)$ and $P_{cs}(4459)$ as the $[\Xi_c \bar{D}]^{1/2^-}$ and $[\Xi_c \bar{D}^*]^{1/2^-}$ ($[\Xi_c \bar{D}^*]^{3/2^-}$) molecular states, the degeneracy of the $[\Xi_c \bar{D}^*]^{1/2^-}$ and $[\Xi_c \bar{D}^*]^{3/2^-}$ channels is removed by the couple-channel effects and recoil corrections.

Another novel phenomenon from the $M_{J/\Psi\Lambda}$ invariant spectrum [1] is that there seems to be a structure around $M = 4254$ MeV. To understand this signal, the LHCb checked the $m(J/\Psi\Lambda)$ distribution close to the $\Lambda_c^+ D_s^-$ threshold and found that this signal is not statistically significant. Nevertheless, the authors in Ref. [21] investigated the $P_{cs}(4338)$

and $P_{cs}(4255)$ pole positions from a unitary $\Xi_c \bar{D} - \Lambda_c \bar{D}_s$ coupled-channel scattering amplitude. Besides, the $P_{cs}(4255)$ pole was also found in a model with the coupling between the meson-baryon molecule and the compact five-quark state [22]. The $P_{cs}(4255)$ state was also suggested in an effective field theory framework [23].

The analogy between the observed ($P_c(4312)$, $P_c(4440)$, $P_c(4457)$) [24, 25] and ($P_{cs}(4338)$, $P_{cs}(4459)$) states are discussed in Ref. [26–28]. However, since the Σ_c and Ξ_c belong to different $SU(3)_f$ multiplets, the relations between the discussed P_c and P_{cs} states are not clear. Besides, the $P_{\Psi ss}^N$ pentaquark states as the partners of the P_c and P_{cs} states are investigated in Ref. [29].

If the P_{cs} states and P_c states can be related via $SU(3)_f$ symmetry, it is important to investigate the similarities and differences between these two sets of molecular candidates. In Ref. [30, 31], we discussed the symmetry properties of different heavy flavor molecular systems via a quark level Lagrangian. We proposed that the interactions of different heavy flavor molecules can be related via a generalized flavor-spin symmetry [30]. This framework provides a suitable tool to discuss the similarities between the P_c and P_{cs} states.

We also notice an important difference between the P_c and P_{cs} states. The minimal quark components of the P_c and P_{cs} states are $c\bar{c}nnn$ and $c\bar{c}nns$ ($n = u, d$), respectively. For the charmed/charmed-strange mesons and baryons, the $SU(3)_f$ symmetry breaking effects are reflected on their physical masses, and we need to distinguish the s quark from u , d quarks when we study the P_{cs} systems. Unlike the P_c pentaquarks, the P_{cs} states can couple to two sets of channels, i.e., the $cns\text{-}\bar{c}n$ type and $cnn\text{-}\bar{c}s$ type channels. In Table I, we list the possible open-charm channels and their thresholds for the P_c and P_{cs} systems.

In this work, we will take the $P_{cs}(4338)$ as a molecular candidate and discuss the following three issues:

- (1) Can we understand the minor binding energy of the $P_{cs}(4338)$ (close to the $\Xi_c \bar{D}$ threshold) through a $\Xi_c \bar{D} - \Lambda_c \bar{D}_s$ coupled-channel effect?
- (2) Can we produce a $P_{cs}(4254)$ bound state by including the $\Xi_c \bar{D} - \Lambda_c \bar{D}_s$ coupled-channel effect with the potential constrained from $SU(3)_f$ symmetry?
- (3) What is the correspondence between the P_c and P_{cs} states if the interactions of the P_c and P_{cs} states obey a generalized flavor-spin symmetry?

* chen_k10@pku.edu.cn

† lzy_15@pku.edu.cn

‡ zhushi@pku.edu.cn

TABLE I. The thresholds of the meson-baryon channels associated with the P_c and P_{cs} systems, we adopt the isospin averaged masses for the ground charmed mesons and baryons [32]. All values are in units of MeV.

P_c		P_{cs}	
$\Lambda_c \bar{D}$	4153.7	$\Lambda_c \bar{D}_s$	4255.5
$\Lambda_c \bar{D}^*$	4295.0	$\Lambda_c \bar{D}_s^*$	4398.7
$\Sigma_c \bar{D}$	4320.8	$\Sigma_c \bar{D}_s$	4422.5
$\Sigma_c^* \bar{D}$	4385.4	$\Sigma_c^* \bar{D}_s$	4487.1
$\Sigma_c \bar{D}^*$	4462.1	$\Sigma_c \bar{D}_s^*$	4565.7
$\Sigma_c^* \bar{D}^*$	4526.7	$\Sigma_c^* \bar{D}_s^*$	4630.3
		$\Xi_c \bar{D}$	4336.7
		$\Xi_c \bar{D}^*$	4478.0
		$\Xi_c' \bar{D}$	4446.0
		$\Xi_c' \bar{D}^*$	4513.2
		$\Xi_c'' \bar{D}^*$	4587.4
		$\Xi_c'' \bar{D}^*$	4654.5

This paper is organized as follows. We present our theoretical framework in Sec. II and the corresponding numerical results and discussions in Sec. III. Sec. IV is the summary.

II. FRAMEWORK

In Ref. [31], we proposed an isospin criterion and pointed out that the P_c and P_{cs} states with the lowest isospin numbers are more likely to form bound states. Based on the same Lagrangian, we only focus on the P_c and P_{cs} states with isospin numbers $I = 1/2$ and 0, respectively. Thus, we will not include the $\Sigma_c^{(*)} \bar{D}_s^{(*)}$ channels listed in Table I for the P_{cs} system.

For the $I = 1/2$ P_c states, we consider the following channels for the $J = 1/2$ and $3/2$ states

$$J = \frac{1}{2} : \Lambda_c \bar{D}, \Lambda_c \bar{D}^*, \Sigma_c \bar{D}, \Sigma_c \bar{D}^*, \Sigma_c^* \bar{D}^*, \quad (3)$$

$$J = \frac{3}{2} : \Lambda_c \bar{D}^*, \Sigma_c^* \bar{D}, \Sigma_c \bar{D}^*, \Sigma_c^* \bar{D}^*. \quad (4)$$

Similarly, for the $I = 0$ P_{cs} states, we include the following channels for the $J = 1/2$ and $3/2$ states

$$J = \frac{1}{2} : \Lambda_c \bar{D}_s, \Lambda_c \bar{D}_s^*, \Xi_c \bar{D}, \Xi_c \bar{D}^*, \Xi_c' \bar{D}, \Xi_c' \bar{D}^*, \Xi_c'' \bar{D}^*, \quad (5)$$

$$J = \frac{3}{2} : \Lambda_c \bar{D}_s^*, \Xi_c \bar{D}^*, \Xi_c' \bar{D}, \Xi_c' \bar{D}^*, \Xi_c'' \bar{D}^*. \quad (6)$$

The result of the P_c (P_{cs}) state with $J = 5/2$ can be obtained from a single-channel calculation and was predicted in Ref. [31] in the same framework. Thus, we will not discuss them further in this work.

A. Lagrangians for the baryon-meson systems

To describe the S -wave interactions between the ground charmed/charmed-strange baryons and mesons, we introduce the following quark-level Lagrangian [4, 31, 33, 34]

$$\mathcal{L} = g_s \bar{q} S q + g_a \bar{q} \gamma_\mu \gamma^5 \mathcal{A}^\mu q. \quad (7)$$

Here, $q = (u, d, s)$, g_s and g_a are two independent coupling constants that describe the interactions from the exchanges of the scalar and axial-vector meson currents. They encode the nonperturbative low energy dynamics of the considered heavy flavor meson-baryon systems.

From this Lagrangian, the effective potential of the light quark-quark interactions reads

$$\mathcal{V} = \tilde{g}_s \boldsymbol{\lambda}_1 \cdot \boldsymbol{\lambda}_2 + \tilde{g}_a \boldsymbol{\lambda}_1 \cdot \boldsymbol{\lambda}_2 \boldsymbol{\sigma}_1 \cdot \boldsymbol{\sigma}_2. \quad (8)$$

Here,

$$\boldsymbol{\lambda}_1 \cdot \boldsymbol{\lambda}_2 = \lambda_1^8 \lambda_2^8 + \lambda_1^i \lambda_2^i + \lambda_1^j \lambda_2^j, \quad (9)$$

i and j sum from 1 to 3 and 4 to 7, respectively. The operators $\lambda_1^8 \lambda_2^8$ ($\lambda_1^8 \lambda_2^8 (\boldsymbol{\sigma}_1 \cdot \boldsymbol{\sigma}_2)$), $\lambda_1^i \lambda_2^i$ ($\lambda_1^i \lambda_2^i (\boldsymbol{\sigma}_1 \cdot \boldsymbol{\sigma}_2)$), and $\lambda_1^j \lambda_2^j$ ($\lambda_1^j \lambda_2^j (\boldsymbol{\sigma}_1 \cdot \boldsymbol{\sigma}_2)$) arise from the exchanges of the isospin singlet, triplet, and two doublets light scalar (axial-vector) meson currents, respectively. The redefined coupling constants are $\tilde{g}_s \equiv g_s^2/m_S^2$ and $\tilde{g}_a \equiv g_a^2/m_A^2$.

The Lagrangian in Eq. (7) allows the exchanges of two types of scalar and axial-vector mesons that have quantum numbers $I(J^P) = 0(0^+)$, $1(0^+)$, $1/2(0^+)$ and $I(J^P) = 0(1^+)$, $1(1^+)$, $1/2(1^+)$, respectively. At present, we can not specifically pin down the coupling parameter of each exchanged meson in the above six meson currents. Alternatively, since the mesons in each meson current have identical interacting Lorentz structure, we use the coupling constant \tilde{g}_s (\tilde{g}_a) to collectively absorb the total dynamical effects from the exchange of each scalar (axial-vector) meson current. In addition, the couplings \tilde{g}_s (\tilde{g}_a) for the scalar (axial-vector) meson currents with different isospin numbers are the same in the SU(3) limit.

The effective potential between the i -th baryon-meson channel $B_i M_i$ and the j -th baryon-meson channel $B_j M_j$ with total isospin I and total angular momentum J can be calculated as

$$v_{ij} = \langle [B_i M_i]_J^I | \mathcal{V} | [B_j M_j]_J^I \rangle. \quad (10)$$

Here, the $|[B_i M_i]_J^I\rangle$ is the quark-level flavor-spin wave function of the considered i -th channel baryon-meson system

$$\begin{aligned} |[B_i M_i]_J^I \rangle &= \sum_{m_{I_1}, m_{I_2}} C_{I_1, m_{I_1}; I_2, m_{I_2}}^{I, I_z} \phi_{I_1, m_{I_1}}^{B_{if}} \phi_{I_2, m_{I_2}}^{M_{if}} \\ &\otimes \sum_{m_{S_1}, m_{S_2}} C_{S_1, m_{S_1}; S_2, m_{S_2}}^{J, J_z} \phi_{S_1, m_{S_1}}^{B_{is}} \phi_{S_2, m_{S_2}}^{M_{is}}. \end{aligned} \quad (11)$$

In Eq. (11), the $\phi_{S_1, m_{S_1}}^{B_{is}}$ and $\phi_{S_2, m_{S_2}}^{M_{is}}$ are the spin wave functions of the baryon and meson, respectively. The total spin wave function can be obtained with the help of SU(2) CG coefficient $C_{S_1, m_{S_1}; S_2, m_{S_2}}^{J, J_z}$. For the flavor wave functions of the considered baryons ($\phi_{I_1, m_{I_1}}^{B_{if}}$) and mesons ($\phi_{I_2, m_{I_2}}^{M_{if}}$), their explicit forms have been given in Ref. [30]. When constructing the total flavor wave functions of the considered baryon-meson systems, we use the SU(2) CG coefficient and take the s quark as a flavor singlet.

The coupled-channel Lippmann-Schwinger equation (LSE) reads

$$\mathbb{T}(E) = \mathbb{V} + \mathbb{V}\mathbb{G}(E)\mathbb{T}(E), \quad (12)$$

with

$$\mathbb{V} = \begin{pmatrix} v_{11} & \cdots & v_{1i} & \cdots & v_{1n} \\ \vdots & & \vdots & & \vdots \\ v_{j1} & \cdots & v_{ji} & \cdots & v_{jn} \\ \vdots & & \vdots & & \vdots \\ v_{n1} & \cdots & v_{ni} & \cdots & v_{nn} \end{pmatrix}, \quad (13)$$

$$\mathbb{T}(E) = \begin{pmatrix} t_{11}(E) & \cdots & t_{1i}(E) & \cdots & t_{1n}(E) \\ \vdots & & \vdots & & \vdots \\ t_{j1}(E) & \cdots & t_{ji}(E) & \cdots & t_{jn}(E) \\ \vdots & & \vdots & & \vdots \\ t_{n1}(E) & \cdots & t_{ni}(E) & \cdots & t_{nn}(E) \end{pmatrix}, \quad (14)$$

and

$$\mathbb{G}(E) = \text{diag} \{G_1(E), \cdots, G_i(E), \cdots, G_n(E)\}. \quad (15)$$

Here,

$$G_i = \frac{1}{2\pi^2} \int dq \frac{q^2}{E - \sqrt{m_{i1}^2 + q^2} - \sqrt{m_{i2}^2 + q^2}} u^2(\Lambda). \quad (16)$$

The m_{i1} and m_{i2} are the masses of the baryon and meson in the i -th channel, respectively. In our previous work [30, 31], we use a step function to exclude the contributions from higher momenta to perform the single-channel calculation. In the coupled-channel case, we need to further suppress the contributions from the channels that are far away from the thresholds of the considered channels. Thus, we introduce a dipole form factor $u(\Lambda) = (1 + q^2/\Lambda^2)^{-2}$ with regular parameter $\Lambda = 1.0 \text{ GeV}$ [21, 35, 36].

The pole position of Eq. (12) satisfies $\|\mathbf{1} - \mathbb{V}\mathbb{G}\| = 0$. For the bound state below the lowest channel, we search the bound state solution in the first Riemann sheet of the lowest channel. For the quasi-bound state between the thresholds of the i -th and j -th channels, we adopt the complex scaling method and replace the integration variable q by $q \rightarrow q \times \exp(-i\theta)$ and maintain $0 < \theta < \pi/2$ to find the quasi-bound state solution in the first Riemann sheet of the higher j -th channel and the second Riemann sheet of the lower i -th channel. [37].

III. NUMERICAL RESULTS

A. Determination of \tilde{g}_s and \tilde{g}_a

We first determine the parameters \tilde{g}_s and \tilde{g}_a in our model. We collect the matrix elements of $\langle \lambda_1 \cdot \lambda_2 \rangle$, $\langle \lambda_1 \cdot \lambda_2 \sigma_1 \cdot \sigma_2 \rangle$ for the P_c and P_{cs} states in Tables II and III, respectively.

We can directly obtain the effective potentials associated with the P_c and P_{cs} states from Tables II and III, respectively.

For example, the explicit form of the effective potential matrix for the $J = 3/2$ P_c states is

$$\mathbb{V}_{3/2}^{P_c} = \begin{pmatrix} \frac{2}{3}\tilde{g}_s & -2\sqrt{3}\tilde{g}_a & 2\tilde{g}_a & 2\sqrt{5}\tilde{g}_a \\ -2\sqrt{3}\tilde{g}_a & -\frac{10}{3}\tilde{g}_s & -\frac{10}{3\sqrt{3}}\tilde{g}_a & -\frac{10\sqrt{\frac{5}{3}}}{3}\tilde{g}_a \\ 2\tilde{g}_a & -\frac{10}{3\sqrt{3}}\tilde{g}_a & -\frac{10}{3}\tilde{g}_s - \frac{20}{9}\tilde{g}_a & \frac{10\sqrt{5}}{9}\tilde{g}_a \\ 2\sqrt{5}\tilde{g}_a & -\frac{10\sqrt{\frac{5}{3}}}{3}\tilde{g}_a & \frac{10\sqrt{5}}{9}\tilde{g}_a & -\frac{10}{3}\tilde{g}_s + \frac{20}{9}\tilde{g}_a \end{pmatrix}. \quad (17)$$

Similarly, the effective potential matrixes $\mathbb{V}_{1/2}^{P_c}$, $\mathbb{V}_{1/2}^{P_{cs}}$, and $\mathbb{V}_{3/2}^{P_{cs}}$ can also be obtained directly from Table II and III.

We use the masses of the observed P_c states as input to determine the coupling constants \tilde{g}_s and \tilde{g}_a . In our previous work, we find that the Lagrangian in Eq. (7) can give a satisfactory description of the observed T_{cc} [38, 39], P_c , and P_{cs} states if we assign the $P_c(4440)$ and $P_c(4457)$ as the $I(J^P) = 1/2(1/2^-)$ and $1/2(3/2^-)$ states. For consistency, we still adopt this set of assignments and use the masses of the $P_c(4440)$ and $P_c(4457)$ as inputs. In the coupled-channel formalism, the bound/quasi-bound states in the $J^P = 1/2^-$ and $3/2^-$ P_c systems satisfy the following equations

$$\text{Re} \left\| \mathbf{1} - \mathbb{V}_{1/2}^{P_c} \mathbb{G}_{1/2}^{P_c} \right\| = 0, \quad (18)$$

$$\text{Im} \left\| \mathbf{1} - \mathbb{V}_{1/2}^{P_c} \mathbb{G}_{1/2}^{P_c} \right\| = 0, \quad (19)$$

$$\text{Re} \left\| \mathbf{1} - \mathbb{V}_{3/2}^{P_c} \mathbb{G}_{3/2}^{P_c} \right\| = 0, \quad (20)$$

$$\text{Im} \left\| \mathbf{1} - \mathbb{V}_{3/2}^{P_c} \mathbb{G}_{3/2}^{P_c} \right\| = 0. \quad (21)$$

These four equations can be solved numerically and we get

$$\tilde{g}_s = 8.28 \text{ GeV}^{-2}, \quad \tilde{g}_a = -1.46 \text{ GeV}^{-2}. \quad (22)$$

The imaginary part of the pole positions of the $P_c(4440)$ and $P_c(4457)$ can also be obtained from Eqs. (18-21).

B. Flavor-spin symmetry of the P_c and P_{cs} systems in the single-channel formalism

With the determined parameters \tilde{g}_s and \tilde{g}_a , we first present our single-channel results for the considered P_c and P_{cs} systems and demonstrate that we can relate the P_c and P_{cs} systems from their interactions constrained by the SU(3) and heavy quark symmetries.

Although the $\Xi_c \bar{D}$ and $\Sigma_c \bar{D}$ belong to different multiplets, in Ref. [30] we proposed that there exists a generalized flavor-spin symmetry between two-body heavy-flavor systems. For two different heavy-flavor meson-baryon systems, if they both possess the same flavor ($\langle H_1^f H_2^f | \lambda_1 \cdot \lambda_2 | H_1^f H_2^f \rangle$) and spin ($\langle H_1^s H_2^s | \sigma_1 \cdot \sigma_2 | H_1^s H_2^s \rangle$) matrix elements, they will still have identical effective potentials in the SU(3) and heavy quark limits.

TABLE II. The matrix elements of $[\langle \lambda_1 \cdot \lambda_2 \rangle, \langle \lambda_1 \cdot \lambda_2 \sigma_1 \cdot \sigma_2 \rangle]$ for the meson-baryon channels associated with the $J^P = 1/2^-$ and $3/2^-$ P_c systems.

$\mathbb{V}_{1/2}^{P_c}$						$\mathbb{V}_{3/2}^{P_c}$				
Channel	$\Lambda_c \bar{D}$	$\Lambda_c \bar{D}^*$	$\Sigma_c \bar{D}$	$\Sigma_c \bar{D}^*$	$\Sigma_c^* \bar{D}^*$	Channel	$\Lambda_c \bar{D}^*$	$\Sigma_c^* \bar{D}$	$\Sigma_c \bar{D}^*$	$\Sigma_c^* \bar{D}^*$
$\Lambda_c \bar{D}$	$[\frac{2}{3}, 0]$	$[0, 0]$	$[0, 0]$	$[0, 2\sqrt{3}]$	$[0, 2\sqrt{6}]$	$\Lambda_c \bar{D}^*$	$[\frac{2}{3}, 0]$	$[0, -2\sqrt{3}]$	$[0, 2]$	$[0, 2\sqrt{5}]$
$\Lambda_c \bar{D}^*$		$[\frac{2}{3}, 0]$	$[0, 2\sqrt{3}]$	$[0, -4]$	$[0, 2\sqrt{2}]$	$\Sigma_c^* \bar{D}$		$[-\frac{10}{3}, 0]$	$[0, -\frac{10}{3\sqrt{3}}]$	$[0, -\frac{10\sqrt{5}}{3}]$
$\Sigma_c \bar{D}$			$[-\frac{10}{3}, 0]$	$[0, -\frac{20}{3\sqrt{3}}]$	$[0, \frac{10\sqrt{2}}{3}]$	$\Sigma_c \bar{D}^*$			$[-\frac{10}{3}, -\frac{20}{9}]$	$[0, \frac{10\sqrt{5}}{9}]$
$\Sigma_c \bar{D}^*$				$[-\frac{10}{3}, \frac{40}{9}]$	$[0, \frac{10\sqrt{2}}{9}]$	$\Sigma_c^* \bar{D}^*$				$[-\frac{10}{3}, \frac{20}{9}]$
$\Sigma_c^* \bar{D}^*$					$[-\frac{10}{3}, \frac{50}{9}]$					

 TABLE III. The matrix elements of $[\langle \lambda_1 \cdot \lambda_2 \rangle, \langle \lambda_1 \cdot \lambda_2 \sigma_1 \cdot \sigma_2 \rangle]$ for the meson-baryon channels associated with the $J^P = 1/2^-$ and $3/2^-$ P_{cs} systems.

$\mathbb{V}_{1/2}^{P_{cs}}$								$\mathbb{V}_{3/2}^{P_{cs}}$					
Channel	$\Lambda_c \bar{D}_s$	$\Lambda_c \bar{D}_s^*$	$\Xi_c \bar{D}$	$\Xi_c \bar{D}^*$	$\Xi_c' \bar{D}$	$\Xi_c' \bar{D}^*$	$\Xi_c^* \bar{D}^*$	Channel	$\Lambda_c \bar{D}_s^*$	$\Xi_c \bar{D}^*$	$\Xi_c^* \bar{D}$	$\Xi_c' \bar{D}^*$	$\Xi_c^* \bar{D}^*$
$\Lambda_c \bar{D}_s$	$[-\frac{4}{3}, 0]$	$[0, 0]$	$[2\sqrt{2}, 0]$	$[0, 0]$	$[0, 0]$	$[0, 2\sqrt{2}]$	$[0, 4]$	$\Lambda_c \bar{D}_s^*$	$[-\frac{4}{3}, 0]$	$[2\sqrt{2}, 0]$	$[0, -2\sqrt{2}]$	$[0, 2\sqrt{\frac{2}{3}}]$	$[0, 2\sqrt{\frac{10}{3}}]$
$\Lambda_c \bar{D}_s^*$		$[-\frac{4}{3}, 0]$	$[0, 0]$	$[2\sqrt{2}, 0]$	$[0, 2\sqrt{2}]$	$[0, -4\sqrt{\frac{2}{3}}]$	$[0, \frac{4}{\sqrt{3}}]$	$\Xi_c \bar{D}^*$		$[-\frac{10}{3}, 0]$	$[0, -2]$	$[0, \frac{2}{\sqrt{3}}]$	$[0, 2\sqrt{\frac{5}{3}}]$
$\Xi_c \bar{D}$			$[-\frac{10}{3}, 0]$	$[0, 0]$	$[0, 0]$	$[0, 2]$	$[0, 2\sqrt{2}]$	$\Xi_c^* \bar{D}$			$[-\frac{10}{3}, 0]$	$[0, -\frac{10}{3\sqrt{3}}]$	$[0, -\frac{10\sqrt{5}}{3}]$
$\Xi_c \bar{D}^*$				$[-\frac{10}{3}, 0]$	$[0, 2]$	$[0, -\frac{4}{\sqrt{3}}]$	$[0, 2\sqrt{\frac{2}{3}}]$	$\Xi_c' \bar{D}^*$				$[-\frac{10}{3}, -\frac{20}{9}]$	$[0, \frac{10\sqrt{5}}{9}]$
$\Xi_c' \bar{D}$					$[-\frac{10}{3}, 0]$	$[0, -\frac{20}{3\sqrt{3}}]$	$[0, \frac{10\sqrt{2}}{3}]$	$\Xi_c^* \bar{D}^*$					$[-\frac{10}{3}, \frac{20}{9}]$
$\Xi_c' \bar{D}^*$						$[-\frac{10}{3}, \frac{40}{9}]$	$[0, \frac{10\sqrt{2}}{9}]$						
$\Xi_c^* \bar{D}^*$							$[-\frac{10}{3}, \frac{50}{9}]$						

In the single-channel formalism, we present the masses and binding energies of the P_c and P_{cs} states in Table IV. The theoretical uncertainties are introduced by considering the experimental errors of the masses of the $P_c(4440)$ and $P_c(4457)$. We collect the P_c and P_{cs} states that share identical effective potentials in the same row. As listed in Table IV, the P_c and P_{cs} states have similar binding energies in the same row and can be related via a flavor-spin symmetry.

C. The masses of P_c states in the multi-channel formalism

Then we explore how the coupled-channel effect influences the masses of the P_c states. As can be seen from Eq. (8), the effective potential consists of two parts, i.e., the central term ($\tilde{g}_s \lambda_1 \cdot \lambda_2$) and the spin-spin interaction ($\tilde{g}_a \lambda_1 \cdot \lambda_2 \sigma_1 \cdot \sigma_2$) term. Since the determined \tilde{g}_s is much larger than \tilde{g}_a , the central term dominates the total effective potential, and therefore determines whether the considered system can form a bound state.

As given in Table II, for the matrix elements in the P_c system, all the diagonal matrix elements have central terms, and some of them have corrections from the spin-spin interaction terms. The off-diagonal terms only consist of the spin-spin interaction terms. Thus, before we perform a practical multi-channel calculation of the P_c system, we may anticipate that

the coupled-channel effect would have small corrections to the masses of the P_c states.

As discussed in Sec. II, we include five and four channels to study the $J = 1/2$ and $J = 3/2$ P_c states, respectively. For the $J = 1/2$ channels, according to their thresholds, we consider five energy regions

$$E \leq m_{\Lambda_c \bar{D}}, \quad (23)$$

$$m_{\Lambda_c \bar{D}} < E \leq m_{\Lambda_c \bar{D}^*}, \quad (24)$$

$$m_{\Lambda_c \bar{D}^*} < E \leq m_{\Sigma_c \bar{D}}, \quad (25)$$

$$m_{\Sigma_c \bar{D}} < E \leq m_{\Sigma_c \bar{D}^*}, \quad (26)$$

$$m_{\Sigma_c \bar{D}^*} < E \leq m_{\Sigma_c^* \bar{D}^*}. \quad (27)$$

We search the bound (quasi-bound) state solutions below the higher threshold in each energy region on the first Riemann sheet. The bound (quasi-bound) state solutions of the $J = 3/2$ P_c , $J = 1/2$ and $3/2$ P_{cs} states can be found by repeating the same procedure. We present the obtained P_c states in Table V. We do not find any bound states below the $\Lambda_c \bar{D}$ threshold. Thus, all the obtained resonances (E_R) listed in Table V should refer to quasi-bound states and have imaginary parts ($\text{Im}(E_R)$). Since we only include the two body open-charm decay channels, the estimated widths (Γ) in Table V are smaller than experimental widths. By comparing the masses of P_c states in Table IV and V, we find that the coupled-channel effect indeed have small influences to the masses of the P_c states.

TABLE IV. In the single-channel formalism, the binding energies of the P_c and P_{cs} states that share the same effective potentials in the SU(3) and heavy quark limits. All results are in units of MeV.

P_c	Mass	BE	P_{cs}	Mass	BE	V
$[\Sigma_c \bar{D}]^{\frac{1}{2}}$	$4312.7^{+4.1}_{-2.6}$	$-8.1^{+4.1}_{-2.6}$	$[\Xi_c \bar{D}]^{\frac{1}{2}}$	$4328.5^{+4.1}_{-2.7}$	$-8.2^{+4.1}_{-2.7}$	$-\frac{10}{3}\tilde{g}_s$
			$[\Xi_c \bar{D}^*]^{\frac{1}{2}, \frac{3}{2}}$	$4468.3^{+4.5}_{-2.9}$	$-9.7^{+4.5}_{-2.9}$	
$[\Sigma_c^* \bar{D}]^{\frac{3}{2}}$	$4376.9^{+4.2}_{-2.7}$	$-8.5^{+4.2}_{-2.7}$	$[\Xi_c' \bar{D}]^{\frac{1}{2}}$	$4437.2^{+4.5}_{-2.8}$	$-8.8^{+4.3}_{-2.8}$	
			$[\Xi_c^* \bar{D}]^{\frac{3}{2}}$	$4503.9^{+4.4}_{-2.8}$	$-9.3^{+4.4}_{-2.8}$	
$[\Sigma_c \bar{D}^*]^{\frac{1}{2}}$	$4438.9^{+4.9}_{-8.9}$	$-23.2^{+4.9}_{-8.9}$	$[\Xi_c' \bar{D}^*]^{\frac{1}{2}}$	$4562.9^{+2.8}_{-9.1}$	$-24.5^{+2.8}_{-9.1}$	$-\frac{10}{3}\tilde{g}_s + \frac{40}{9}\tilde{g}_a$
$[\Sigma_c \bar{D}^*]^{\frac{3}{2}}$	$4457.5^{+3.7}_{-1.8}$	$-4.6^{+3.7}_{-1.8}$	$[\Xi_c' \bar{D}^*]^{\frac{3}{2}}$	$4582.2^{+4.0}_{-2.0}$	$-5.2^{+4.0}_{-2.0}$	$-\frac{10}{3}\tilde{g}_s - \frac{20}{9}\tilde{g}_a$
$[\Sigma_c^* \bar{D}^*]^{\frac{1}{2}}$	$4498.8^{+6.6}_{-6.0}$	$-27.9^{+6.6}_{-6.0}$	$[\Xi_c^* \bar{D}^*]^{\frac{1}{2}}$	$4625.3^{+6.8}_{-12.7}$	$-29.2^{+6.8}_{-12.7}$	$-\frac{10}{3}\tilde{g}_s + \frac{50}{9}\tilde{g}_a$
$[\Sigma_c^* \bar{D}^*]^{\frac{3}{2}}$	$4510.3^{+4.1}_{-4.1}$	$-16.4^{+4.1}_{-4.1}$	$[\Xi_c^* \bar{D}^*]^{\frac{3}{2}}$	$4637.9^{+4.3}_{-4.2}$	$-16.6^{+4.3}_{-4.2}$	$-\frac{10}{3}\tilde{g}_s + \frac{20}{9}\tilde{g}_a$

TABLE V. The results of P_c states obtained in the coupled-channel formalism. Here, $\Gamma = -2\text{Im}(E_R)$, all the results are in units of MeV.

Our		Exp			
State	J^P	Mass	Γ	Mass	Width
$P_c(4312)$	$\frac{1}{2}^-$	$4308.2^{+2.6}_{-4.5}$	$2.6^{+2.4}_{-1.7}$	$4311.9^{+7.0}_{-0.9}$	10 ± 5
$P_c(4440)$	$\frac{1}{2}^-$	$4440.3^{+4.0}_{-5.0}$ (input)	$9.8^{+4.6}_{-5.8}$	$4440.3^{+4.0}_{-5.0}$	21^{+10}_{-11}
$P_c(4457)$	$\frac{3}{2}^-$	$4457.7^{+4.0}_{-1.8}$ (input)	$2.0^{+1.4}_{-0.8}$	$4457.3^{+4.0}_{-1.8}$	$6.4^{+6.0}_{-2.8}$
$P_c(4380)$	$\frac{3}{2}^-$	$4373.3^{+3.4}_{-6.8}$	$5.2^{+20.2}_{-3.5}$	—	—
$P_c(4500)$	$\frac{1}{2}^-$	$4501.4^{+5.0}_{-6.2}$	$8.8^{+17.2}_{-5.4}$	—	—
$P_c(4510)$	$\frac{3}{2}^-$	$4513.4^{+5.8}_{-3.1}$	$7.6^{+9.4}_{-0.0}$	—	—

D. A numerical experiment on the $(\Lambda_c \bar{D}_s^{(*)}, \Xi_c \bar{D}^{(*)})$ coupled-channel systems

There exists an important difference between the effective potential matrices in the P_c and P_{cs} systems. As presented in Tables II and III, the diagonal matrix elements in the P_{cs} system are very similar to those of the P_c system. But for the off-diagonal matrix elements, the effective potentials of the $\Lambda_c \bar{D}_s - \Xi_c \bar{D}$ and $\Lambda_c \bar{D}_s^* - \Xi_c \bar{D}^*$ channels in the P_{cs} system with $J = 1/2$ or $3/2$ consist of central terms. These terms may give considerable corrections to the spectrum of the P_{cs} states.

For the $J = 1/2$ and $J = 3/2$ P_{cs} systems, as given in Eq. (5-6) we need to perform seven and five coupled-channel calculations. Before we perform such complete calculations, we first perform a detailed discussion on the $(\Lambda_c \bar{D}_s, \Xi_c \bar{D})$ and $(\Lambda_c \bar{D}_s^*, \Xi_c \bar{D}^*)$ coupled-channel systems.

The effective potential matrixes of the $J = 1/2$ $(\Lambda_c \bar{D}_s, \Xi_c \bar{D})$, $(\Lambda_c \bar{D}_s^*, \Xi_c \bar{D}^*)$ systems, and the $J = 3/2$ $(\Lambda_c \bar{D}_s^*, \Xi_c \bar{D}^*)$ system share the same expressions in the heavy quark limit. From Table III, we obtain the corresponding effective potential matrix

$$\mathbb{V} = \begin{pmatrix} v_{11} & v_{12} \\ v_{21} & v_{22} \end{pmatrix} \quad (28)$$

with

$$v_{11} = -\frac{4}{3}\tilde{g}_s, \quad v_{22} = -\frac{10}{3}\tilde{g}_s, \quad (29)$$

$$v_{12} = v_{21} = 2\sqrt{2}\tilde{g}_s g_x. \quad (30)$$

Here, for the diagonal matrix elements listed in Table II and III, their dominant components are from the exchange of the non-strange light scalar meson currents. Since the interactions of the off-diagonal channel $\Lambda_c \bar{D}_s^{(*)} - \Xi_c \bar{D}^{(*)}$ are introduced via the exchange of the strange scalar meson currents, we further introduce a factor g_x to estimate the SU(3) breaking effects. Compared with the exchange of the non-strange light scalar meson currents, the off-diagonal matrix elements should be suppressed by the mass of strange mesons. Thus, we assume $0 \leq g_x \leq 1$. This factor also reflects the coupling strength of the $\Lambda_c \bar{D}_s - \Xi_c \bar{D}$ channel. With $g_x = 0$, the $\Lambda_c \bar{D}_s^{(*)}$ does not couple to the $\Xi_c \bar{D}^{(*)}$ channel. With $g_x = 1.0$, the $\Lambda_c \bar{D}_s^{(*)}$ couples to the $\Xi_c \bar{D}^{(*)}$ channel and its coupling strength is set to be the value in the SU(3) limit.

In Fig. 1 (b), we present the variation of the masses for the bound states $P_{cs}(4338)$ and $P_{cs}(4255)$ as the parameter g_x increases. The masses of the $P_{cs}(4338)$ and $P_{cs}(4255)$ are denoted with black lines. At $g_x = 0$, the $\Lambda_c \bar{D}_s$ channel itself has a weak attractive force $v_{11} = -4/3\tilde{g}_s$, and this force is too weak to form a $\Lambda_c \bar{D}_s$ bound state. On the contrary, the $\Xi_c \bar{D}$ channel can form a bound state and its mass is about $M = 4329$ MeV, slightly smaller than the experimental value. As the g_x increases, the attractive force of the $P_{cs}(4338)$ decreases and its mass moves closer to the $\Xi_c \bar{D}$ threshold. In a very narrow region $0.62 \leq g_x \leq 0.64$, the attractive force is just enough to form a $P_{cs}(4338)$ bound state at the $\Xi_c \bar{D}$ threshold and the weak attractive channel $\Lambda_c \bar{D}_s$ starts to form a bound state due to the $\Xi_c \bar{D} - \Lambda_c \bar{D}_s$ coupling. Only in this very narrow region, the $P_{cs}(4338)$ and $P_{cs}(4255)$ can coexist as quasi-bound states. At $g_x > 0.64$, the $\Xi_c \bar{D} - \Lambda_c \bar{D}_s$ coupling further weakens the attractive force of the $\Xi_c \bar{D}$ channel and the $P_{cs}(4338)$ no longer exists as a quasi-bound state, while the attractive force of the $\Lambda_c \bar{D}_s$ channel becomes stronger and its mass will decrease. The observation of the $P_{cs}(4338)$ by LHCb seems to exclude the parameter region $0.64 < g_x < 1.0$.

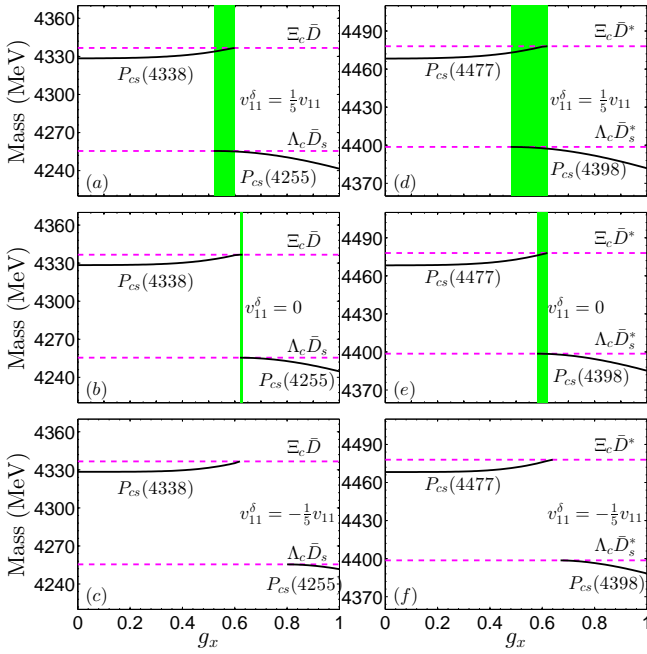


FIG. 1. The variations of the masses for the possible bound states in the $(\Lambda_c \bar{D}_s^{(*)} \Xi_c \bar{D}^{(*)})$ two-channel system as the parameter g_x increases. We use the blue-dotted lines to denote the $\Lambda_c \bar{D}_s^{(*)}$ and $\Xi_c \bar{D}^{(*)}$ thresholds. The masses of the P_{cs} states are denoted with black lines. Figs. (a), (d), Figs. (b), (e), and Figs. (c), (f) are obtained at $v_{11}^\delta = 1/5 v_{11}$, 0, and $-1/5 v_{11}$, respectively. The green bands in Figs. (a), (d), (b), (e) denote that the bound states near the $\Lambda_c \bar{D}_s$ ($\Lambda_c \bar{D}_s^*$) and $\Xi_c \bar{D}$ ($\Xi_c \bar{D}^*$) thresholds can coexist in this g_x region.

Here, we also check the pole position of the $P_{cs}(4338)$ at $g_x > 0.64$ in the energy region slightly above the $\Xi_c \bar{D}$ threshold. We find that the pole of the $P_{cs}(4338)$ still exists in the first Riemann sheet. This is mainly due to the fact that the $\Lambda_c \bar{D}_s - \Xi_c \bar{D}$ coupling leads the $P_{cs}(4338)$ to be a state that have a considerable width, thus the central value of the $P_{cs}(4338)$ mass may cross the $\Xi_c \bar{D}$ threshold. In this case, the $P_{cs}(4338)$ should be interpreted as a quasi-bound state above the $\Xi_c \bar{D}$ threshold. Nevertheless, in this work, we restrict our scope to the case that the masses of the bound/quasi-bound states are below their corresponding thresholds.

To understand why the g_x region that allows the $P_{cs}(4338)$ and $P_{cs}(4255)$ states to coexist is so narrow, we further check the role of the $\Lambda_c \bar{D}_s$ channel in our two-channel model. We allow the effective potential of the $\Lambda_c \bar{D}_s$ channel to have a 20% shift, i.e.,

$$v'_{11} = v_{11} + v_{11}^\delta, \quad v_{11}^\delta = 0, \pm \frac{1}{5} v_{11}, \quad (31)$$

and further check how the masses of the $P_{cs}(4338)$ and $P_{cs}(4255)$ change as we increase the g_x .

The channel $\Lambda_c \bar{D}_s$ itself has a weak attractive force, as presented in Fig. 1 (a), at $g_x = 0$. After we increase this force by 20%, this single-channel still can not form a bound state. But the g_x region that allows these two P_{cs} states to coexist becomes broader. On the contrary, as illustrated in Fig. 1 (c), if

we decrease the attractive force of the $\Lambda_c \bar{D}_s$ channel by 20%, the $P_{cs}(4338)$ and $P_{cs}(4255)$ can not coexist no matter how we adjust the off-diagonal $\Lambda_c \bar{D}_s - \Xi_c \bar{D}$ coupling. Thus, the narrow g_x region that the $P_{cs}(4338)$ and $P_{cs}(4255)$ can coexist is due to the fact that the $\Lambda_c \bar{D}_s$ channel has a small but non-negligible attractive force.

The results for the $J = 1/2$ and $3/2$ ($\Lambda_c \bar{D}_s^*, \Xi_c \bar{D}^*$) coupled-channels are presented in Fig. 1 (d-f). We find that the roles of the predicted $P_{cs}(4477)$ and $P_{cs}(4398)$ with $J^P = 1/2^-$ or $3/2^-$ are very similar to those of the $P_{cs}(4338)$ and $P_{cs}(4255)$ with $J^P = 1/2^-$, respectively.

E. The results of P_{cs} system in the coupled-channel formalism

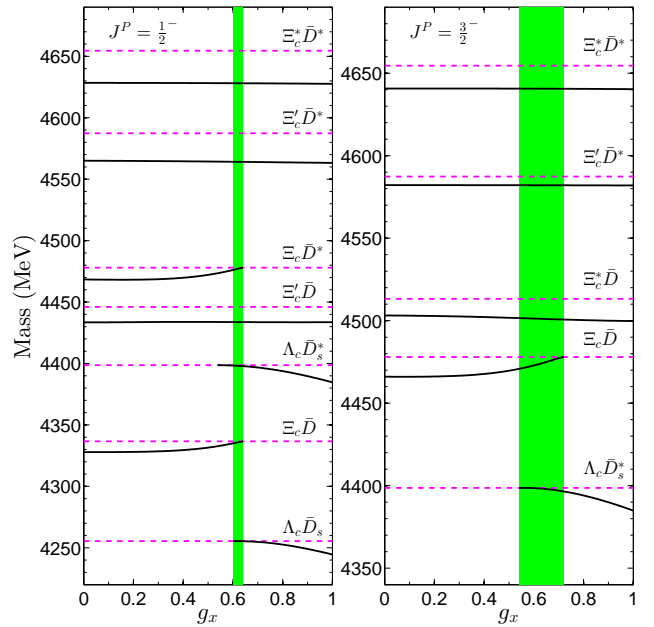


FIG. 2. The variations of the masses for the P_{cs} states with $J^P = 1/2^-$ and $J^P = 3/2^-$ as the g_x increases. We use the blue-dotted lines to denote the considered meson-baryon thresholds. The masses of the obtain bound states are denoted with black lines. The green bands denote that the bound states near the $\Lambda_c \bar{D}_s^{(*)}$ or $\Xi_c \bar{D}^{(*)}$ thresholds can coexist in this g_x region.

We present our complete multi-channel calculations on the $J = 1/2$ and $J = 3/2$ P_{cs} systems in Fig. 2. We find that only the bound states close to the $\Lambda_c \bar{D}_s^{(*)}$ and $\Xi_c \bar{D}^{(*)}$ channels have significant dependence on the g_x , since these bound states can couple to the $\Lambda_c \bar{D}_s^{(*)}$ and $\Xi_c \bar{D}^{(*)}$ channels through non-negligible central terms, while the bound states that can only couple to the $\Lambda_c \bar{D}_s^{(*)}$ and $\Xi_c \bar{D}^{(*)}$ channels via the spin-spin interaction terms have very tiny dependence on the parameter g_x .

To further present our numerical results, we fix the parameter g_x at 0.5 and 0.62. We denote these two cases as case 1 and case 2. The case 1 and case 2 correspond to the results that the

possible $P_{cs}(4255)$ signal does not/does exist. The results of these two cases are listed in Table VI.

Comparing the masses of the P_{cs} states calculated in the single-channel formalism (Table IV) with the results obtained in the coupled-channel formalism (Table VI), we infer that the off-diagonal channels that only consist of the spin-spin interaction terms have small influence on the masses of the P_{cs} states, which is very similar to the P_c system. From Table VI, we find that there exist three extra P_{cs} states below the $\Lambda_c \bar{D}_s^{(*)}$ thresholds in the case 2.

For the $P_{cs}(4338)$ state, due to its strong coupling to the $\Lambda_c \bar{D}_s$ channel, the width of this state is broader than the result given by LHCb. Note that in our calculation, we only include the open-charm two body meson-baryon channels. Thus, the width predicted by our model should be regarded as the lower limit of the experimental width. Since the $P_{cs}(4338)$ is reported in the $B \rightarrow J/\Psi \Lambda \bar{p}$ channel, the narrow width of the $P_{cs}(4338)$ found by the LHCb may be due to the small phase space of this B meson decay process. Thus, confirming the $P_{cs}(4338)$ in other decay processes is important to pin down its resonance parameters.

Besides, we also find that the P_{cs} states that are close to the $\Xi_c \bar{D}^{(*)}$ states are broader than the other P_{cs} states due to its strong coupling to the $\Lambda_c \bar{D}_s^{(*)}$ channel. Thus, our results suggest that there exist two $J^P = 1/2^-$ and $J^P = 3/2^-$ quasi-bound states near the $\Xi_c \bar{D}^*$ region. This region is close to the reported $P_{cs}(4459)$, and the two-peak structure in this region has been discussed in many literatures [4, 8, 13, 40, 41]. The results from our model provide a new possibility, i.e., the two P_{cs} structures in this region may have a significant overlap in the $J/\Psi \Lambda$ invariant spectrum due to their considerable widths. The decay behaviors of the $P_{cs}(4459)$ have been discussed in Refs. [11, 29, 42–44]. The decay widths and decay patterns are valuable in identifying the structure of the $P_{cs}(4459)$. Further investigations on the total and partial decay widths will be crucial to accomplish a thorough understanding on the P_c and P_{cs} states.

F. The correspondence between the P_c and P_{cs} systems

Finally, we compare the masses of the P_c and P_{cs} states obtained from our multi-channel model. Since the mass of constituent s quark is heavier than that of the u, d quarks by about 100 MeV. Thus, we shift the mass plot of the P_{cs} system by 100 MeV to check the similarities between the P_c and P_{cs} states. We present the multi-channel results for the P_c system in Fig. 3 (a), and the multi-channel results for the P_{cs} system calculated at $g_x = 0.5$ and $g_x = 0.62$ are given in Fig. 3 (b). As can be seen from Fig. 3 (a) and (b), the meson-baryon thresholds in the P_c and P_{cs} systems have the following analogies

$$m_{\Lambda_c \bar{D}^{(*)}} \leftrightarrow m_{\Lambda_c \bar{D}_s^{(*)}}, \quad (32)$$

$$m_{\Sigma_c^{(*)} \bar{D}^{(*)}} \leftrightarrow m_{\Xi_c'^{(*)} \bar{D}^{(*)}}. \quad (33)$$

We denote these thresholds with the blue-dotted lines in Fig. 3. Besides, there exist two extra meson-baryon thresholds

$\Xi_c \bar{D}$ and $\Xi_c \bar{D}^*$ in the P_{cs} system. These two channels can not directly correspond to the meson-baryon channels in the P_c system. We denote these two thresholds with the green-dotted lines.

As can be seen from Fig. 3, there exist six P_c states with $J^P = 1/2^-$ or $3/2^-$. These six states can correspond to the six states in the P_{cs} system. We denote the masses of the central values of these 12 states with black lines and their uncertainties are denoted with green rectangles. According to Fig. 3, the experimentally observed P_c states and the predicted P_{cs} states should have the following analogies

$$P_c(4312) \leftrightarrow P_{cs}(4434), \quad (34)$$

$$P_c(4440) \leftrightarrow P_{cs}(4564), \quad (35)$$

$$P_c(4457) \leftrightarrow P_{cs}(4582). \quad (36)$$

As indicated in Fig. 3, if we replace the $\Lambda_c \bar{D}_s^*$ and $\Xi_c' \bar{D}$ channels with the $\Xi_c \bar{D}$ and $\Xi_c \bar{D}^*$ channels, respectively, we can reluctantly obtain the following analogies

$$P_c(4312) \leftrightarrow P_{cs}(4472), \quad (37)$$

$$P_c(4440) \leftrightarrow P_{cs}(4564), \quad (38)$$

$$P_c(4457) \leftrightarrow P_{cs}(4582). \quad (39)$$

The predicted $P_{cs}(4472)$ may correspond to the reported $P_{cs}(4459)$. However, such an analogy indicates a considerable SU(3) breaking effect. In both sets of analogies, the $P_{cs}(4338)$ can not directly correspond to the lowest $P_c(4312)$ state.

There exist three and six extra P_{cs} states that can not correspond to the states in the P_c system at $g_x = 0.50$ and $g_x = 0.62$, respectively. We denote the masses of the central values of these states with the black lines and their uncertainties are denoted with red rectangles. Further experimental explorations on the P_{cs} system may help us to distinguish which case should be preferred.

IV. SUMMARY

Motivated by the recently discovered $P_{cs}(4338)$ from the LHCb Collaboration, we have performed a multi-channel calculation of the $I = 1/2$ P_c and $I = 0$ P_{cs} systems and presented a comparison between the interactions of the P_c and P_{cs} states in the SU(3)_f limit and heavy quark limit.

Unlike the $\bar{c}n - cnn$ ($n = u, d$) type meson-baryon channels in the P_c system, we need to consider two types of channels when we study the P_{cs} system, i.e., the $\bar{c}n - cns$ and $\bar{c}s - cnn$ meson-baryon channels. This difference will lead to extra states in the P_{cs} systems.

The effective potentials of the P_c and P_{cs} states are collectively obtained via a quark-level Lagrangian, which allows us to construct the correspondence between the P_c and P_{cs} systems.

We use the masses of the $P_c(4440)$ and $P_c(4457)$ as input to determine the coupling parameters \tilde{g}_s and \tilde{g}_a in our model. We first study the masses of the P_c states in the single-channel and coupled-channel formalisms. Since all the off-diagonal

TABLE VI. The results of the P_{cs} states calculated at $g_x = 0.50$ and $g_x = 0.62$ in the coupled-channel formalism. All results are in units of MeV.

States	$g_x = 0.50$			$g_x = 0.62$		
	Mass	Γ	BE	Mass	Γ	BE
$[\Lambda_c \bar{D}_s]_{\frac{1}{2}^-}$	—	—	—	$4255.5_{-0.7}^{+0.0}$	0.0	$-0.0_{-0.7}^{+0.0}$
$[\Lambda_c \bar{D}_s^*]_{\frac{1}{2}^-}$	—	—	—	$4398.1_{-1.5}^{+0.2}$	0.0	$-0.6_{-1.5}^{+0.2}$
$[\Lambda_c \bar{D}_s^*]_{\frac{3}{2}^-}$	—	—	—	$4398.3_{-1.3}^{+0.4}$	0.0	$-0.4_{-1.3}^{+0.4}$
$[\Xi_c \bar{D}]_{\frac{1}{2}^-}$	$4331.6_{-1.5}^{+2.6}$	$17.8_{-7.6}^{+3.6}$	$-5.0_{-1.5}^{+2.6}$	$4335.9_{-2.1}^{+0.7}$	$26.0_{-10.2}^{+5.0}$	$-0.7_{-2.1}^{+0.7}$
$[\Xi_c \bar{D}^*]_{\frac{1}{2}^-}$	$4472.1_{-1.6}^{+2.5}$	$23.4_{-6.0}^{+5.2}$	$-5.9_{-1.6}^{+2.5}$	$4477.1_{-0.8}^{+0.5}$	$33.0_{-8.0}^{+6.0}$	$-0.9_{-0.8}^{+0.5}$
$[\Xi_c \bar{D}^*]_{\frac{3}{2}^-}$	$4469.7_{-6.6}^{+1.9}$	$14.6_{-10.6}^{+4.4}$	$-8.3_{-6.6}^{+1.9}$	$4473.7_{-8.7}^{+2.7}$	$20.2_{-13.6}^{+5.8}$	$-4.7_{-8.7}^{+2.7}$
$[\Xi_c' \bar{D}]_{\frac{1}{2}^-}$	$4433.8_{-4.8}^{+3.4}$	$0.8_{-0.6}^{+5.0}$	$-12.2_{-4.8}^{+3.4}$	$4433.7_{-5.2}^{+3.5}$	$0.4_{-0.0}^{+2.6}$	$-12.3_{-5.2}^{+3.5}$
$[\Xi_c' \bar{D}]_{\frac{3}{2}^-}$	$4501.8_{-3.4}^{+4.4}$	$7.7_{-5.1}^{+22.3}$	$-11.4_{-3.4}^{+4.4}$	$4501.2_{-3.7}^{+4.2}$	$7.8_{-5.3}^{+25.4}$	$-12.0_{-3.7}^{+4.2}$
$[\Xi_c' \bar{D}^*]_{\frac{1}{2}^-}$	$4564.4_{-4.0}^{+3.4}$	$4.5_{-2.7}^{+9.5}$	$-23.0_{-4.0}^{+3.4}$	$4564.1_{-7.4}^{+3.3}$	$4.8_{-2.8}^{+9.2}$	$-23.3_{-7.4}^{+3.3}$
$[\Xi_c' \bar{D}^*]_{\frac{3}{2}^-}$	$4582.1_{-2.0}^{+4.3}$	$1.9_{-1.1}^{+0.7}$	$-5.3_{-2.0}^{+4.3}$	$4582.1_{-2.0}^{+4.2}$	$2.0_{-1.2}^{+1.3}$	$-5.3_{-2.0}^{+4.2}$
$[\Xi_c^* \bar{D}^*]_{\frac{1}{2}^-}$	$4628.2_{-7.1}^{+3.5}$	$5.0_{-3.0}^{+9.0}$	$-26.3_{-7.1}^{+3.5}$	$4628.1_{-7.3}^{+5.1}$	$5.2_{-3.2}^{+24.5}$	$-26.4_{-7.3}^{+5.1}$
$[\Xi_c^* \bar{D}^*]_{\frac{3}{2}^-}$	$4640.7_{-3.2}^{+5.8}$	$7.0_{-0.8}^{+8.2}$	$-13.8_{-3.2}^{+5.8}$	$4640.6_{-3.2}^{+5.9}$	$7.2_{-4.4}^{+8.4}$	$-13.9_{-3.2}^{+5.9}$

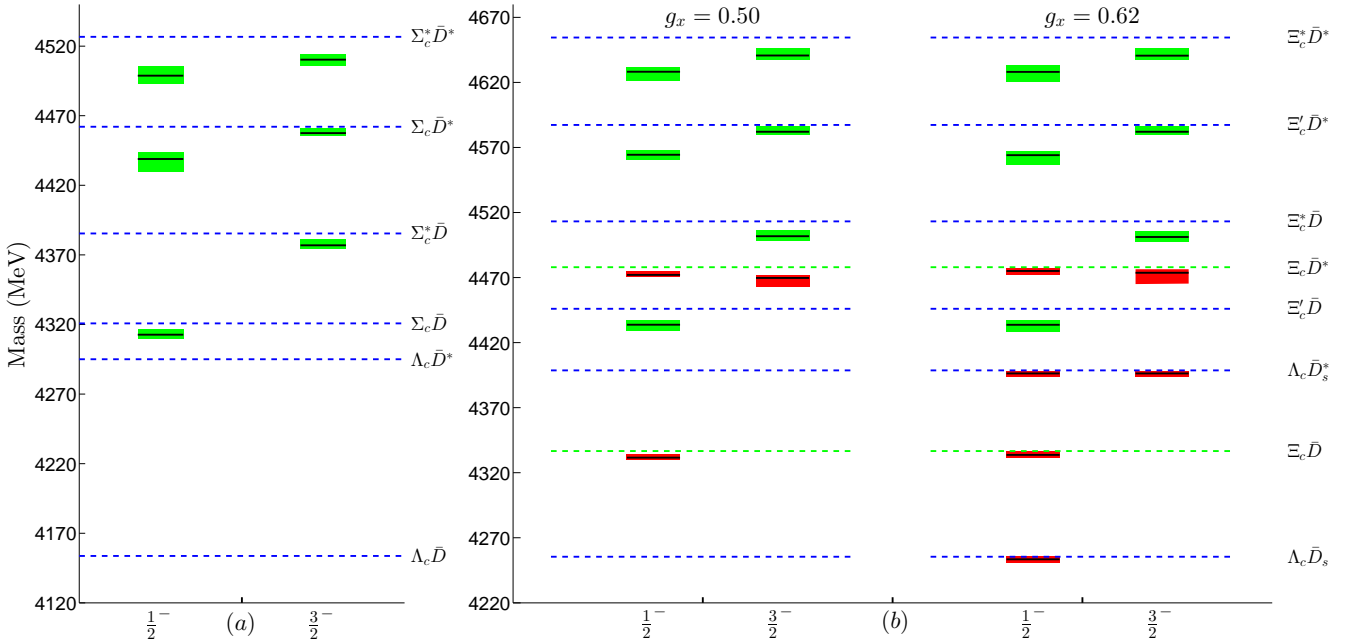


FIG. 3. The mass spectra of the P_c and P_{cs} states in the multi-channel formalism, we present the results of P_{cs} system at $g_x = 0.50$ and $g_x = 0.62$. The meson-baryon thresholds $m_{\Lambda_c \bar{D}^{(*)}}$, $m_{\Lambda_c \bar{D}_s^{(*)}}$, $m_{\Sigma_c^{(*)} \bar{D}^{(*)}}$, $m_{\Xi_c^{(*)} \bar{D}^{(*)}}$ are illustrated with the blue-dotted lines. The two extra thresholds $\Xi_c \bar{D}$ and $\Xi_c \bar{D}^*$ in the P_{cs} system are denoted with the green-dotted lines. We use the black lines to denote the central values of the obtained P_c and P_{cs} states, their uncertainties are illustrated with the green and red rectangles. The six green states in the P_c system can directly correspond to the six green states in the P_{cs} system.

terms in the effective potential matrices consist of the spin-spin interaction terms, the coupled-channel effect provides very small corrections to the masses of the P_c states.

There exists an important difference between the P_c system and P_{cs} system. In the P_{cs} system, the off-diagonal terms

$\Lambda_c \bar{D}_s^{(*)} - \Xi_c \bar{D}^{(*)}$ in the effective potential matrices consist of the central terms and will have considerable corrections to the mass spectrum of the P_{cs} states. To clarify the role of the $\Lambda_c \bar{D}_s^{(*)} - \Xi_c \bar{D}^{(*)}$ coupling, we have performed a numerical

experiment on the $(\Lambda_c \bar{D}_s^{(*)}, \Xi_c \bar{D}^{(*)})$ coupled-channel system. Our results suggest that the mass of the $P_{cs}(4338)$ may shift very close to the $\Xi_c \bar{D}$ threshold by adjusting the coupling between the $\Xi_c \bar{D}$ and $\Lambda_c \bar{D}_s$ channels. This coupling may also lead to a $P_{cs}(4255)$ state in a reasonable g_x region.

Then we present our complete multi-channel calculations of the P_{cs} systems. Since the $P_{cs}(4255)$ is not confirmed by experiment, we present our numerical results with $g_x = 0.50/0.62$, corresponding to the case that the $P_{cs}(4255)$ does not/does exist, respectively. Due to the strong $\Lambda_c \bar{D}_s - \Xi_c \bar{D}$ couplings, our predicted width of $P_{cs}(4338)$ is broader than the experimental value. The reported narrower width may be due to the small phase space of the B meson decay process. Confirming the $P_{cs}(4338)$ state in other processes will be helpful to pin down its resonance parameters. There exist two P_{cs} states with $J^P = 1/2^-$ and $J^P = 3/2^-$ below the $\Xi_c \bar{D}^*$ threshold. The masses of these two states are close to the mass of the reported $P_{cs}(4459)$. Due to the $\Lambda_c \bar{D}_s^* - \Xi_c \bar{D}^*$ coupling, these two states should have considerable widths

and may have significant overlap in the $J/\Psi\Lambda$ invariant spectrum. Further experimental exploration would be important to test our predictions.

Finally, we present a complete correspondence between the P_c and P_{cs} states. The observed $P_c(4312)$, $P_c(4440)$, and $P_c(4457)$ do not directly correspond to the observed $P_{cs}(4338)$ and $P_{cs}(4459)$. It is particularly interesting to find the SU(3) P_{cs} states that may correspond to the observed P_c states, and to investigate if such a correspondence does exist. Further experimental researches on these topics will be helpful to fulfill a complete picture on the spectra of the P_c and P_{cs} systems.

ACKNOWLEDGMENTS

This research is supported by the National Science Foundation of China under Grants No. 11975033, No. 12070131001 and No. 12147168.

-
- [1] LHCb, [arXiv:2210.10346 \[hep-ex\]](#).
[2] L. Meng, B. Wang and S. L. Zhu, [arXiv:2208.03883 \[hep-ph\]](#).
[3] R. Aaij *et al.* [LHCb], *Sci. Bull.* **66**, 1278-1287 (2021).
[4] B. Wang, L. Meng and S. L. Zhu, *Phys. Rev. D* **101**, no.3, 034018 (2020).
[5] F. Z. Peng, M. J. Yan, M. Sánchez Sánchez and M. P. Valderrama, *Eur. Phys. J. C* **81**, no.7, 666 (2021).
[6] R. Chen, *Phys. Rev. D* **103**, no.5, 054007 (2021).
[7] M. Z. Liu, Y. W. Pan and L. S. Geng, *Phys. Rev. D* **103**, no.3, 034003 (2021).
[8] C. W. Xiao, J. J. Wu and B. S. Zou, *Phys. Rev. D* **103**, no.5, 054016 (2021).
[9] J. J. Wu, R. Molina, E. Oset and B. S. Zou, *Phys. Rev. Lett.* **105**, 232001 (2010).
[10] E. Santopinto and A. Giachino, *Phys. Rev. D* **96**, no.1, 014014 (2017).
[11] C. W. Shen, J. J. Wu and B. S. Zou, *Phys. Rev. D* **100**, no.5, 056006 (2019).
[12] C. W. Xiao, J. Nieves and E. Oset, *Phys. Lett. B* **799**, 135051 (2019).
[13] J. T. Zhu, L. Q. Song and J. He, *Phys. Rev. D* **103**, no.7, 074007 (2021).
[14] H. X. Chen, W. Chen, X. Liu and S. L. Zhu, *Phys. Rept.* **639**, 1-121 (2016).
[15] F. K. Guo, C. Hanhart, U. G. Meißner, Q. Wang, Q. Zhao and B. S. Zou, *Rev. Mod. Phys.* **90**, no.1, 015004 (2018) [erratum: *Rev. Mod. Phys.* **94**, no.2, 029901 (2022)].
[16] Y. R. Liu, H. X. Chen, W. Chen, X. Liu and S. L. Zhu, *Prog. Part. Nucl. Phys.* **107**, 237-320 (2019).
[17] L. Meng, B. Wang, G. J. Wang and S. L. Zhu, [arXiv:2204.08716 \[hep-ph\]](#).
[18] H. X. Chen, W. Chen, X. Liu, Y. R. Liu and S. L. Zhu, [arXiv:2204.02649 \[hep-ph\]](#).
[19] X. K. Dong, F. K. Guo and B. S. Zou, *Progr. Phys.* **41**, 65-93 (2021).
[20] T. J. Burns and E. S. Swanson, [arXiv:2208.05106 \[hep-ph\]](#).
[21] S. X. Nakamura and J. J. Wu, [arXiv:2208.11995 \[hep-ph\]](#).
[22] A. Giachino, A. Hosaka, E. Santopinto, S. Takeuchi, M. Takizawa and Y. Yamaguchi, [arXiv:2209.10413 \[hep-ph\]](#).
[23] M. J. Yan, F. Z. Peng, M. Sánchez Sánchez and M. Pavon Valderrama, [arXiv:2207.11144 \[hep-ph\]](#).
[24] R. Aaij *et al.* [LHCb], *Phys. Rev. Lett.* **122**, no.22, 222001 (2019).
[25] R. Aaij *et al.* [LHCb], *Phys. Rev. Lett.* **115**, 072001 (2015).
[26] M. Karliner and J. L. Rosner, *Phys. Rev. D* **106**, no.3, 036024 (2022).
[27] F. L. Wang and X. Liu, [arXiv:2207.10493 \[hep-ph\]](#).
[28] X. W. Wang and Z. G. Wang, [arXiv:2207.06060 \[hep-ph\]](#).
[29] P. G. Ortega, D. R. Entem and F. Fernandez, [arXiv:2210.04465 \[hep-ph\]](#).
[30] K. Chen, B. Wang and S. L. Zhu, *Phys. Rev. D* **105**, no.9, 096004 (2022).
[31] K. Chen, R. Chen, L. Meng, B. Wang and S. L. Zhu, *Eur. Phys. J. C* **82**, no.7, 581 (2022).
[32] P. A. Zyla *et al.* [Particle Data Group], *PTEP* **2020**, no.8, 083C01 (2020).
[33] B. Wang, L. Meng and S. L. Zhu, *Phys. Rev. D* **101**, no.9, 094035 (2020).
[34] L. Meng, B. Wang and S. L. Zhu, *Phys. Rev. C* **101**, no.6, 064002 (2020).
[35] D. B. Leinweber, A. W. Thomas and R. D. Young, *Phys. Rev. Lett.* **92**, 242002 (2004).
[36] P. Wang, D. B. Leinweber, A. W. Thomas and R. D. Young, *Phys. Rev. D* **75**, 073012 (2007).
[37] Z. W. Liu, J. M. M. Hall, D. B. Leinweber, A. W. Thomas and J. J. Wu, *Phys. Rev. D* **95**, no.1, 014506 (2017).
[38] R. Aaij *et al.* [LHCb], [\[arXiv:2109.01056 \[hep-ex\]\]](#).
[39] R. Aaij *et al.* [LHCb], [\[arXiv:2109.01038 \[hep-ex\]\]](#).
[40] Z. G. Wang, *Int. J. Mod. Phys. A* **36**, no.10, 2150071 (2021).
[41] H. X. Chen, W. Chen, X. Liu and X. H. Liu, *Eur. Phys. J. C* **81**, no.5, 409 (2021).
[42] M. L. Du, Z. H. Guo and J. A. Oller, *Phys. Rev. D* **104**, no.11, 114034 (2021).
[43] K. Azizi, Y. Sarac and H. Sundu, *Phys. Rev. D* **103**, no.9, 094033 (2021).
[44] R. Chen, *Eur. Phys. J. C* **81**, no.2, 122 (2021).